Electronic Supplementary Materials

A novel peroxidase-mimicking Cu, S co-doped carbon dot nanozyme for dual-mode lactate biosensing in serum and sweat

Ali M. Alaseem[a], Glowi Alasiri[b], Razan Orfali[b], Ramadan Ali[c], Al-Montaser Bellah H. Ali[d], Mohamed M. El-Wekil[e*]

[a] Department of pharmacology College of Medicine, Imam Mohammad Ibn Saud Islamic University (IMSIU), Riyadh 13317, Saudi Arabia

[b] Department of Biochemistry, College of Medicine, Imam Mohammad Ibn Saud Islamic University (IMSIU), Riyadh, 13317, Saudi Arabia.

[c] Department of Pharmaceutical Chemistry, Faculty of Pharmacy, University of Tabuk, Tabuk 71491, Saudi Arabia

[d] Department of Pharmaceutical Analytical Chemistry, Faculty of Pharmacy, Assiut University, Assiut, 71526, Egypt

[e] Pharmaceutical Chemistry Department, Faculty of Pharmacy, Badr University in Assiut (BUA), 2014101, Assiut, Egypt

Correspondence

*** mohamed.elwakeel@pharm.aun.edu.eg, mohamed.mohamoud@ymail.com**

Instruments

UV–visible absorption spectra were recorded using a Shimadzu 1601 PC UV–Vis spectrophotometer, whereas the concentrations of Cu were determined by inductively coupled plasma atomic emission spectroscopy (ICP-AES) using a PerkinElmer instrument. Fluorescence excitation and emission spectra were recorded using a Shimadzu RF-5301 PC spectrofluorometer equipped with a quartz cuvette and operated at a slit width of 3 nm. The morphology of the Cu, S@CDs was examined by transmission electron microscopy (TEM) using a JEOL JEM-100CX II instrument. Particle size and polydispersity were determined by dynamic light scattering (DLS) using a Zetasizer Nano ZS instrument. In addition, the elemental composition and surface chemical states of the prepared materials were analyzed by X-ray photoelectron spectroscopy (XPS) with an ESCA ULVAC-PHI 1600 spectrometer. The crystalline structure of the synthesized material was analyzed by powder X-ray diffraction (PXRD) on a PW 1710 diffractometer, while its vibrational characteristics were further investigated by micro-Raman spectroscopy. Surface functional groups were identified by FT-IR using a Nicolet™ iS™10 spectrometer, whereas elemental composition was evaluated by EDX with a NEX QC+ QuantEZ system.

Fluorescence quantum yield measurements of Cu-S@CDs

Quantum yields (Φ_X) were determined relative to quinine sulfate standard (QY = 54% in H_2SO_4 at 310 nm) under identical instrumental settings. To avoid inner-filter effects, sample and reference absorbance values were kept below 0.05 at 315 nm. Emission spectra were integrated over the full fluorescence band (corrected for instrument response), and the following relation was applied:

$$\phi_X = \phi_s \times \frac{F_{Cu-S@CDs}}{F_S} \times \frac{A_S}{A_{Cu-S@CDs}} \times \frac{\eta_{Cu-S@CDs}}{\eta_S}$$

Φ_X represents the quantum yield of Cu-S@CDs, ϕ_S represents the quantum yield of quinine sulfate, F_X is the fluorescence intensity of Cu-S@CDs, F_S is the fluorescence intensity of standard (S, quinine sulfate), A refers to the absorbance value and η refers to the refractive index of the solvent (H_2SO_4). The synthesized Cu-S@CDs were dissolved in distilled water (η = 1.33) and S was dissolved in H_2SO_4 (η = 1.33).

Catalytic kinetics

The catalytic behavior of Cu-S@CDs was evaluated by measuring the absorbance of the oxidized product at 654 nm. Steady-state kinetic studies were carried out under two different substrate regimes: by varying the concentration of H_2O_2 (0.1–2.2 mM) while maintaining the TMB concentration at 12 mM, and by varying the TMB concentration (2–26 mM) at a fixed H_2O_2 concentration of 0.8 mM. The kinetic parameters, namely the Michaelis constant (Km) and maximum reaction velocity (Vmax), were calculated from the Michaelis–Menten equation and corresponding Lineweaver–Burk plots, where V denotes the initial reaction rate and [S] represents the substrate concentration.

$$\mathbf{V = V_{max} \times [S]/(Km + [S])} \qquad \mathbf{(1)}$$

$$\mathbf{1/V = (Km/V_{max})\ (1/[S]) + (1/V_{max})} \qquad \mathbf{(2)}$$

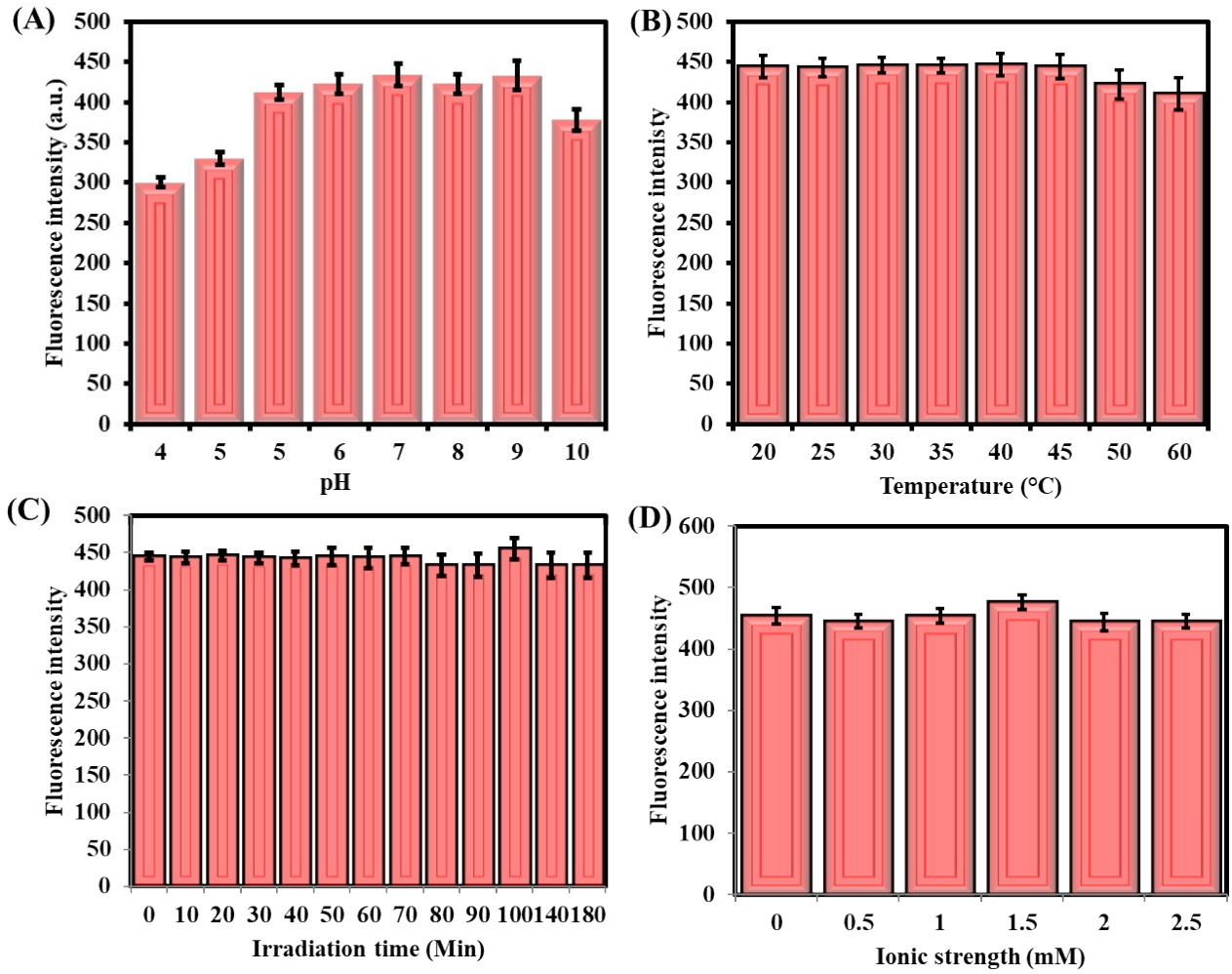

Fig. S1 Stability of Cu-S@CDs under different conditions.

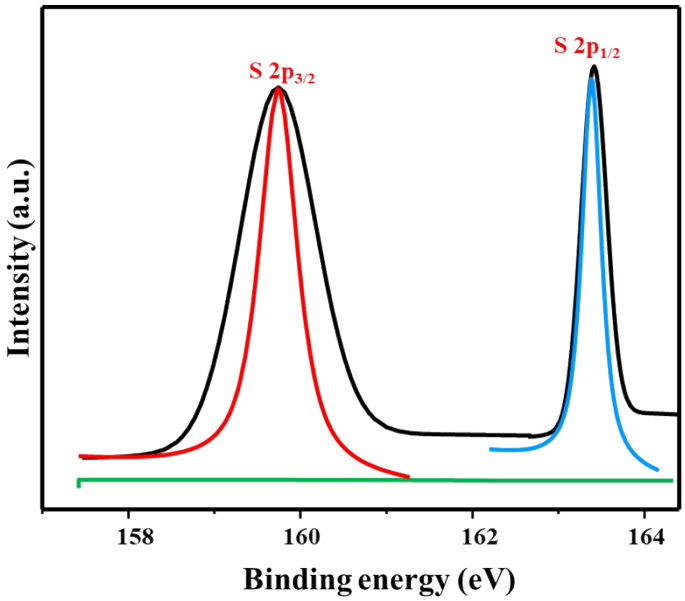

Fig. S2 High resolution spectrum of S 2p.

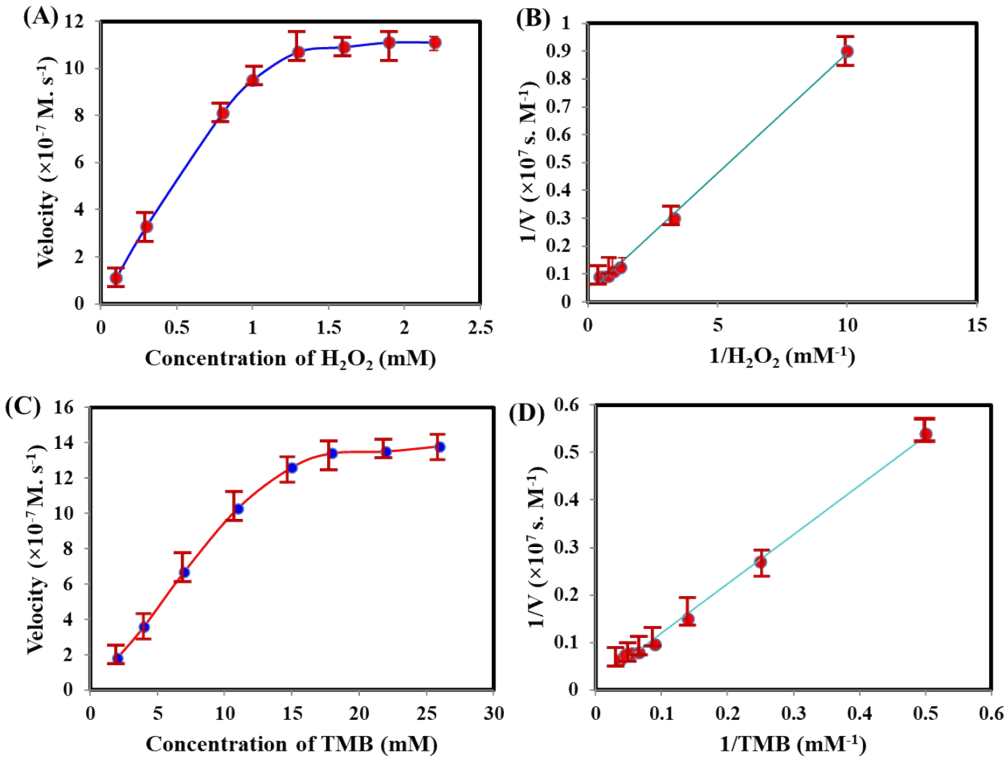

Fig. S3 Steady-state kinetic behavior of Cu-S@CDs analyzed using Michaelis–Menten plots (A, C) and Lineweaver–Burk plots (B, D). Number of replicates for all determinations are four.

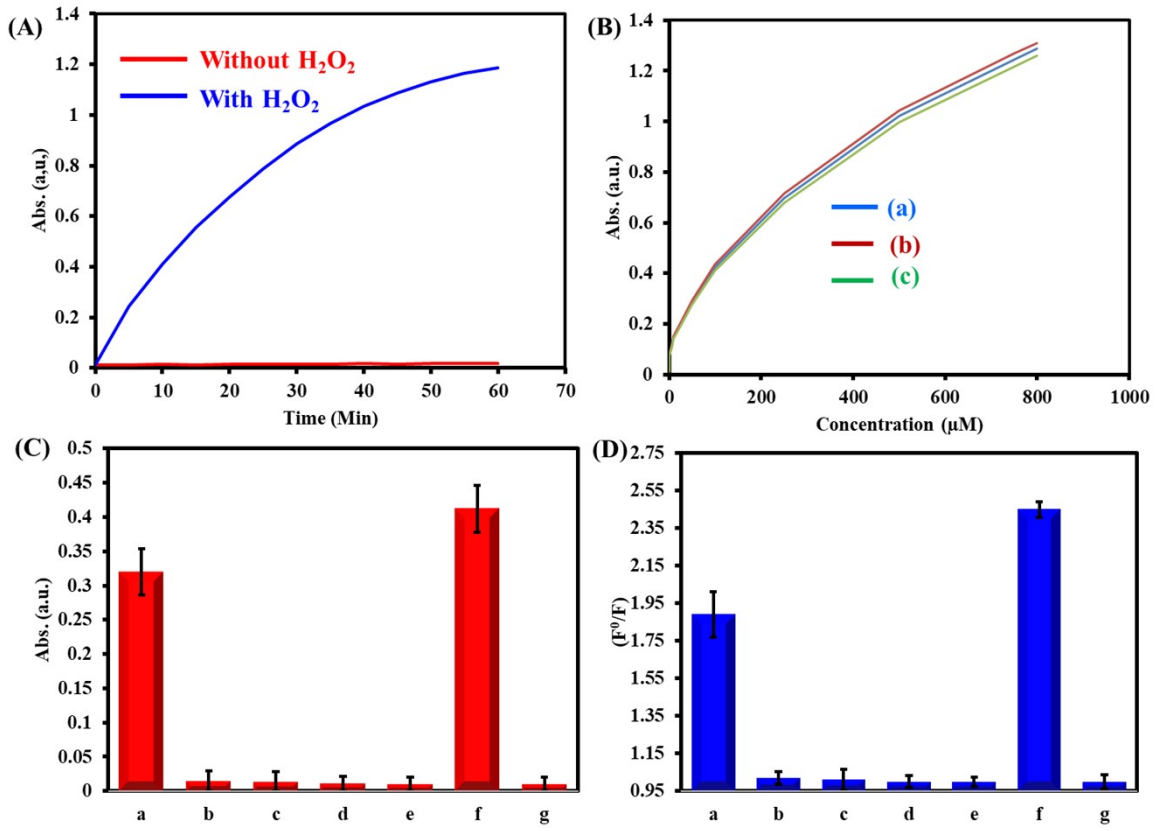

Fig. S4 (A) Time course of absorbance at 512 nm (Cu,S@CDs without H_2O_2); (B) Oxygen dependence – lactate calibration curves under different O_2 conditions (a. Air-saturated: Dissolved O_2 ≈ 250 μM (ambient, no purge), b. O_2-saturated: Purged with pure O_2 for 15 min, ≈ 1200 μM O_2, c. Deoxygenated: Purged with N_2 for 15 min, ≈ 50 μM O_2; (C) Colorimetric and (D) fluorometric component necessity tests (a. Lactate oxidase + lactate + Cu,S@CDs + phenol + 4-aminoantipyrine, b. Lactate oxidase, c. Without lactate, d. Without Cu,S@CDs, e. Without phenol + 4-AAP, e. H_2O_2+Cu,S@CDs + phenol + 4-aminoantipyrine, f. Buffer only.

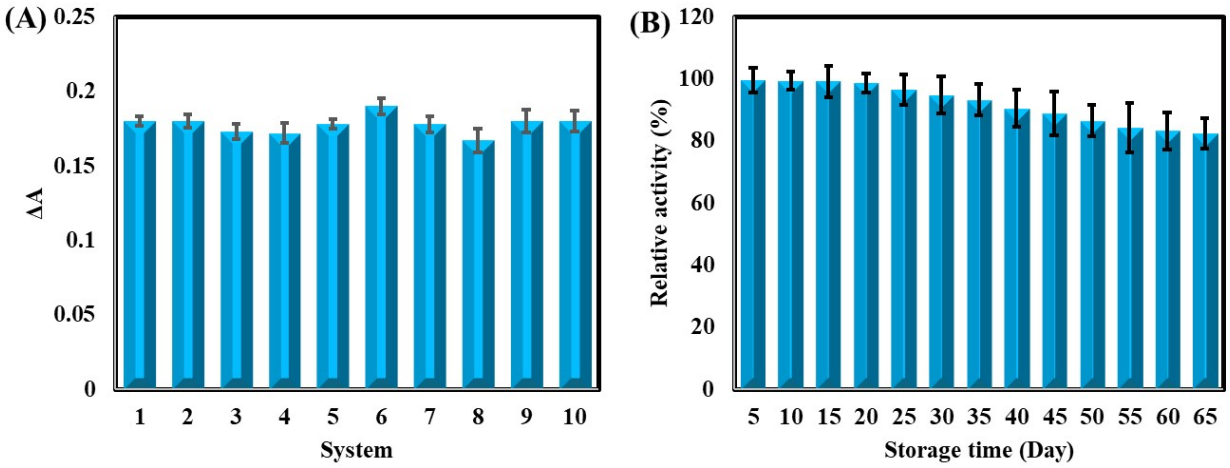

Fig. S5 (A) Reproducibility and (B) stability of the system for measuring 30 μM lactate. Number of replicates are three for all measurements.

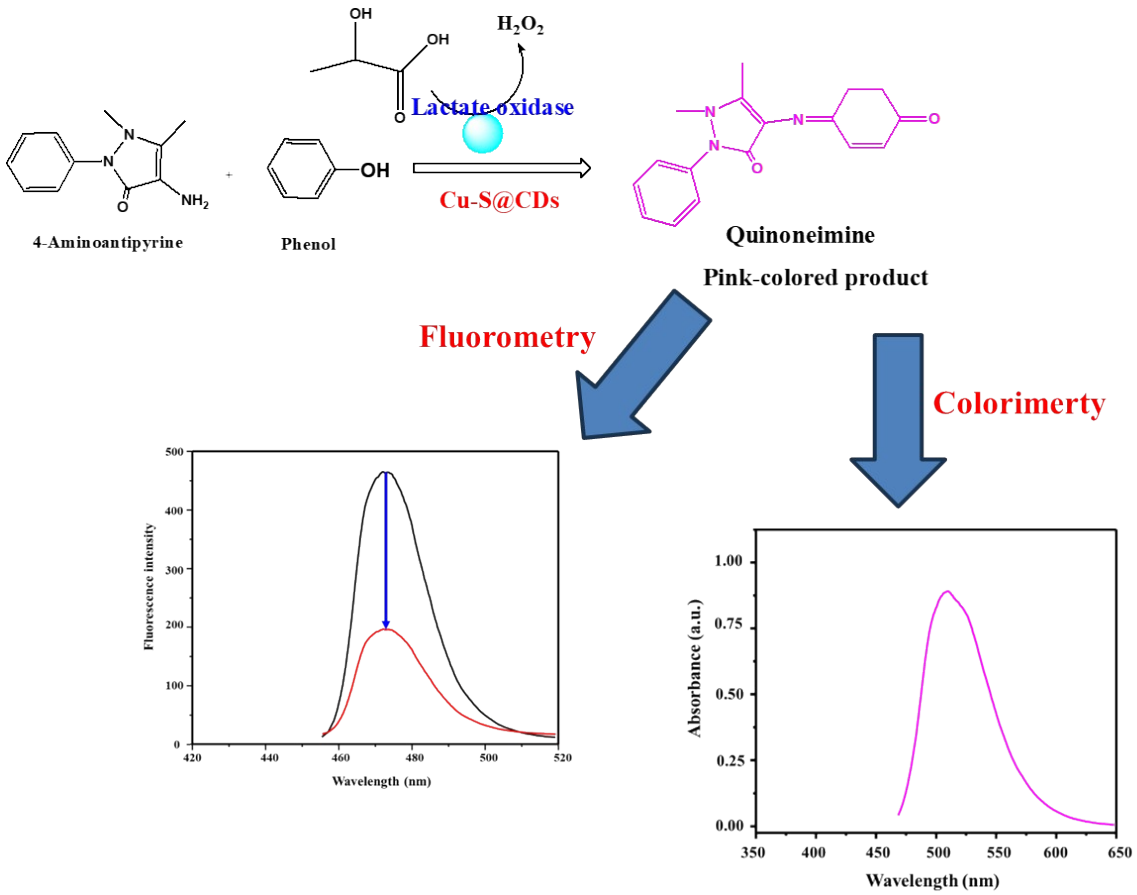

Scheme S1. Proposed dual-mode detection of lactate using Cu-S@CDs-based chromogenic system.

Table S1. Kinetic parameter comparison between Cu-S@CDs and other peroxidase-like catalysts.

Catalyst	K_m (mM)		V_{max} (10^{-8} M s^{-1})		Ref.
	TMB	H_2O_2	TMB	H_2O_2	
Cu-S@CDs	0.121	0.188	18.87	16.68	**This work**
HRP	0.434	3.70	10.00	8.71	[1]
Fe/Eu-MOF	0.115	0.113	1.59	3.82	[2]
Au/MOFs (Fe, Mn)/CNTs	0.34	0.33	3.38	17.65	[3]
2D Ni/Fe MOF	0.411	0.037	12.5	3.30	[4]
Cu-$CuFe_2O_4$	0.69	0.087	16.87	32.18	[5]

Table S2 Steady-state kinetic parameters of Cu,S@CDs and HRP toward TMB and H_2O_2, including turnover number (kcat) and catalytic efficiency (kcat/Km).

Catalyst	Substrate	Km (mM)	Vmax ($\times 10^{-8}$ M·s^{-1})	kcat (s^{-1})	kcat/Km (M^{-1}·s^{-1})
Cu,S@CDs	TMB	0.12	8.45	6.45	5.38×10^4
Cu,S@CDs	H_2O_2	0.08	7.92	6.05	7.56×10^4
HRP	TMB	0.43	0.18	0.14	3.26×10^2

Table S3 Reproducibility of the colorimetric and fluorometric methods (n = 5).

Concentration (µM)	Colorimetric approach			Fluorometric approach		
	Found (µM)	Recovery %	RSD %	Found (µM)	Recovery %	RSD %
5.0	5.23	104.6	3.76	5.30	106.0	3.67
100.0	96.78	96.8	2.78	104.87	104.9	4.08
400.0	405.80	101.5	3.20	394.19	98.5	3.66

Table S4 Analytical performance of the Cu,S@CDs-based assay in buffer, serum, and sweat.

Parameter	Buffer (PBS, pH 7.4)	Human Serum (100× diluted)	Human Sweat (200× diluted)
Linear range (μM)	0.02–800 (fluoro) 0.1–750 (color)	0.05–800 (fluoro) 0.2–750 (color)	0.1–800 (fluoro) 0.2–750 (color)
LOD (μM)	0.0025 (fluoro) 0.022 (color)	0.008 (fluoro) 0.035 (color)	0.015 (fluoro) 0.050 (color)
LOQ (μM)	0.008 (fluoro) 0.07 (color)	0.025 (fluoro) 0.12 (color)	0.050 (fluoro) 0.17 (color)
Slope (calibration)	0.0014 (color) 0.0014 (fluoro)	0.00132 ± 0.00005 (color) 0.00135 ± 0.00004 (fluoro)	0.00128 ± 0.00006 (color) 0.00130 ± 0.00005 (fluoro)
Matrix effect (%)	–	–5.7% (color) –3.6% (fluoro)	–8.6% (color) –7.1% (fluoro)
Intra-day RSD (%)	<3%	<4.5%	<5.5%
Inter-day RSD (%)	<5%	<7%	<8%

Matrix effect (%) = (Slope_matrix / Slope_buffer – 1) × 100

Table S5 Precision data for lactate determination in spiked serum and sweat (n=10).

Matrix	Spiked Lactate (μM)	Found (μM)	Intra-day RSD (%)	Inter-day RSD (%)
Serum (100× diluted)	5.0	4.92 ± 0.18	3.7	5.2
	20.0	19.85 ± 0.52	2.6	4.8
	100.0	99.2 ± 2.8	2.8	5.1
Sweat (200× diluted)	10.0	9.78 ± 0.42	4.3	6.5
	50.0	49.2 ± 2.1	4.3	6.8
	200.0	198.5 ± 8.5	4.3	7.2

Table S6 Correlation with reference method for serum samples (n=10).

Parameter	Colorimetric mode	Fluorometric mode
Regression equation	y = 0.96x + 0.12	y = 0.98x + 0.08
Correlation coefficient (R^2)	0.976	0.989
Bias (%)	–4.2%	–2.1%
p-value (paired t-test)	0.18 (>0.05)	0.32 (>0.05)

Table S7 Comparison with commercial sweat lactate kit (n=10).

Sample	Commercial kit (µM)	Colorimetric (µM)	Fluorometric (µM)
1	15.2 ± 1.1	14.8 ± 0.9	15.0 ± 0.8
2	28.5 ± 2.0	27.9 ± 1.5	28.2 ± 1.3
3	42.1 ± 2.5	41.5 ± 2.0	41.8 ± 1.8
...	...	...	...
Mean bias	–	–4.2%	–2.8%
R^2	–	0.971	0.985

Table S8 Quantitative comparison of single-mode versus dual-mode detection performance for lactate determination in serum and sweat.

Parameter	Colorimetric alone	Fluorometric alone	Dual-mode (consensus)	Improvement
False positive rate (serum, n=50)	8% (4/50)	6% (3/50)	0% (0/50)	100% reduction
False positive rate (sweat, n=50)	12% (6/50)	10% (5/50)	2% (1/50)	83% reduction
Effective dynamic range (μM)	0.1–750	0.02–500*	0.02–750**	30× wider than fluoro alone†
Mean absolute error (serum, n=20)	5.8%	6.9%	2.7%	53–61% reduction
Mean absolute error (sweat, n=20)	7.4%	9.2%	3.4%	54–63% reduction
Outlier detection	No	No	Yes (6/100 flagged)	New capability
Samples requiring re-analysis	Not identified	Not identified	6% (6/100)	Prevents erroneous results

*Fluorometric error exceeds 10% above 500 μM due to inner filter saturation.

**Combined range: use fluorometric for <50 μM, colorimetric for >50 μM.

†Compared to using fluorometric alone for concentrations >50 μM.

References

1. L. Gao, J. Zhuang, L. Nie, J. Zhang, Y. Zhang, N. Gu, T. Wang, J. Feng, D. Yang, S. Perrett, X. Yan, Intrinsic peroxidase-like activity of ferromagnetic nanoparticles, Nature Nanotechnology, 2 (2007) 577-583.
2. W. Shi, T. Li, N. Chu, X. Liu, M. He, B. Bui, M. Chen, W. Chen, Nano-octahedral bimetallic Fe/Eu-MOF preparation and dual model sensing of serum alkaline phosphatase (ALP) based on its peroxidase-like property and fluorescence, Materials Science and Engineering: C, 129 (2021) 112404.
3. X. Dang, H. Zhao, Bimetallic Fe/Mn metal-organic-frameworks and Au nanoparticles anchored carbon nanotubes as a peroxidase-like detection platform with increased active sites and enhanced electron transfer, Talanta, 210 (2020) 120678.
4. Q. Li, Q. Wang, Y. Li, X. Zhang, Y. Huang, 2D bimetallic Ni/Fe MOF nanosheet composites as a peroxidase-like nanozyme for colorimetric assay of multiple targets, Analytical Methods, 13 (2021) 2066-2074.
5. F. Xia, Q. Shi, Z. Nan, Facile synthesis of Cu-$CuFe_2O_4$ nanozymes for sensitive assay of H_2O_2 and GSH, Dalton Transactions, 49 (2020) 12780-12792.